J Mater Sci (2006) 41:6290–6299
DOI 10.1007/s10853-006-0503-z

Metallurgical and electrochemical approach of Pb–(2wt.%)Sm and Pb(0.08wt.%)Ca(2wt.%)Sm lead alloys

A. Maître · M. Vilasi

Received: 14 January 2004 / Accepted: 30 August 2005 / Published online: 12 August 2006

Abstract The metallurgical study of Pb–2wt.%Sm and Pb–0.08wt.%Ca–2wt.%Sm has been performed from hardness measurements, DSC tests, TEM and SEM observations. It has been shown that the binary alloys do not hardened by microprecipitation of an intermetallic phase such as Pb_3Sm: after 2 years, the hardness of Pb–2wt.%Sm alloy is equal to that of pure lead, i.e. 6 HV. Moreover, for Pb–Ca alloy, it appears that the rare earth addition accelerates the three transformations of the ageing. In the simulated overcharge conditions of the acid battery, the Pb–2wt.%Sm grid alloy shows a lower corrosion resistance in 5 M sulphuric acid solution than pure lead. Indeed, the weight loss measured for the binary alloy is increased by 1.5 when it is compared to that of pure lead. This effect is probably due to the grain size decrease and, consequently, to the intergranular corrosion rising for the Pb–0.08%Ca–2.0%Sm with samarium additions in Pb–Ca alloy.

A. Maître (✉)
Laboratoire Science des Procédés Céramiques et Traitements de Surface, UMR CNRS 6638, Faculté des Sciences et Techniques, 123, Avenue Albert-Thomas, F-87060 Limoges Cedex, France
e-mail: alexandre.maitre@unilim.fr

M. Vilasi
Laboratoire de Chimie du Solide Minéral, UMR CNRS 7555, Faculté des Sciences et Techniques, BP 239, Boulevard des Aiguillettes, F-54506 Vandoeuvre-Les-Nancy Cedex, France

Introduction

Since several decades, most manufacturers of lead acid batteries have opted for lead–calcium alloys as the material of choice of the positive grids [1, 2]. Indeed, the use of lead–antimony grid alloys always causes loss of water. In fact, the addition of antimony produces a hydrogen potential increase and so allows the water to electrolyse. So, the lead calcium alloys were used for fabrication of maintenance free batteries. However, lead–calcium alloys always require the addition of a third element such as tin in order to improve their corrosion resistance in overcharge conditions and to avoid the passivation phenomenon in conditions of deep discharge [3, 4].

From metallurgical observations, calorimetric analyses, hardness measurements, several authors [5–7] have shown that the age-hardening of the Pb–Ca alloys exhibits three successive transformations namely:

- a first discontinuous transformation immediately after cooling with a linear movement of reaction fronts through the grain;
- a second discontinuous transformation which is accompanied by an irregular motion of reaction fronts. This step is also called «puzzling». The two first reactions are very rapid and are characterized by low transformation energies;
- a discontinuous or continuous precipitation of Pb_3Ca phase.

The addition of a third element such as tin in lower content, can modify the transformation sequence and inhibits or accelerates the age-hardening kinetic of the Pb–0.08%Ca alloy. Otherwise, the rare earth addition

can improve the mechanical anchorage of corrosion layers as shown for Ni-based alloys during cyclic oxidation tests [8]. This latter effect is particularly interesting for lead alloys because the corrosion layers obtained in concentrated sulphuric acid solution scale off rapidly during potential cycling between the deep discharge and overcharge of the battery [9]. Furthermore, the rare earth additions (e.g. Sm) can lead to the mechanical property improvement by increasing the lattice parameter mismatch between lead matrix (0.495 nm) and the intermetallic precipitated phase (Pb_3Sm: 0.483 nm, Pb_3Ca: 0.493 nm) [10].

Starting materials and experimental procedure

Synthesis of alloys

Specimens of Pb–2wt.%Sm and of Pb–0.112wt.%Ca–2wt.%Sm alloys were synthesised from a Pb–0.12wt.%Ca master alloy, pure lead (99.95%, Goodfellow) and pure samarium (R.O.C., 99.995%). The raw materials were melted in an induction furnace under argon (quality UL', Air Liquide). The final samples of Pb–0.08%Ca–2%Sm were obtained by melting Pb–0.08%Ca2%Sm alloy and pure lead at 800°C for an hour under nitrogen.

The alloys were then cast in an iced aluminium mould. Finally, the specimens were made in the shape of plates (40 mm × 40 mm × 3 mm) or cylinders ($Ø$ = 5 mm, L = 35 mm) for hardness measurements and DSC tests, respectively.

Characterization

Hardness measurements

The ageing kinetic of Pb–0.08wt.%Ca–2wt.%Sm alloys were determined from Vickers hardness measurements (under a loading charge of 20 N) with a macro Vickers hardness tester (Testwell-type). The hardness data were calculated from the average of at least five hardness readings from each sample. The average hardness data were found to be reproducible within 5%.

DSC tests

The main thermal effects accompanying each metallurgical transformation were measured with a microcalorimeter (Sceres-type sensitivity of 10 μW) in the temperature range [−10, 270°C]. The DSC thermograms were obtained by subtracting calorimetric signal of the first heating, which corresponds to transformations with those of the second heating when the sample has reached its thermodynamic equilibrium.

Morphological observations (SEM and TEM studies)

The observation of Pb(–Ca)–Sm alloy microstructure and of the corrosion layers was performed with a scanning electron microscopy (Hitachi-S2500) operating at 15 or 20 kV. This apparatus is equipped with an energy dispersive X-ray spectrometer (EDXS).

Thin foils of lead alloys for transmission electron microscopy study were prepared from an experimental procedure which was developed in our laboratory. Firstly, a small block (4 mm × 3 mm × 12 mm) was cut from the plate core. Secondly, the cutting of foils (with thickness inferior to 5 μm) from this block was performed by microtomy (Microtome Reichert Ultracute apparatus). At last, the argon-ion milling of these foils with a PIPS apparatus (Gatan model 691) permits reaching thickness values included between 10 and 20 nm.

These thin foils were examined in a Philips-CM20 electron microscope operating at 200 kV. This instrument is equipped with an energy dispersive X-ray spectrometer (EDXS) allowing chemical analysis of the precipitates and permits obtaining Small Area Electron Diffraction (SAED) pattern for the phase identification.

Electrochemical tests

The tests were performed in a three-electrode electrochemical cell which was connected to a EG&G Princeton potentiostat driven by a computer. The circular and horizontal working electrode (S = 2.68 cm^2) was placed at the bottom under a Pt-disk electrode, with a reference electrode of K_2SO_4-saturated mercurous sulphate electrode (E = 0.658 V/SHE). The working electrode potentials are always given with respect to this reference electrode. The working electrode was mechanically polished with different grades of SiC papers as follow: 240, 400, 800 and 1200 then with colloidal silica dispersed in water.

The polarisation test at 1.5 V for 5 days at room temperature in 5 M concentrated sulphuric acid solution gives the electrochemical behaviour of lead alloy samples in simulating battery overcharge. After this test, the weight loss was determined by dissolving the corrosion products in hydrazine solution [3].

Electron microprobe

The chemical composition of alloys precipitated intermetallic phase and of corrosion products were

determined by electron microprobe analysis. The apparatus used were CAMECA SX50 and CAMECA SX100, which are equipped with 4 or 5 spectrometers, respectively. The operating conditions were 15 kV accelerating voltage, 10 nA probe current and the size of the excitated zone was about 1 μm^3. Accumulating times on standards and samples were determined in order to define a good accuracy for the element content analysis.

Experimental results and discussions

Sequence of metallurgical transformations

The DSC curve of supersaturated Pb–0.08%Ca–2%Sm alloy (see Fig. 1a) shows the presence of four exothermic heating effects (B–E) whereas the thermogram of the quenched Pb–2 wt.%Sm alloy does not reveal any heating effect. For the ternary alloys, the peaks B and C can be associated to the transformations of the age hardening: the puzzling reaction (B) and the microprecipitation of the hardening phase Pb_3Ca (C). The exothermic effects (D) and (E) correspond to the reprecipitation of the coarse precipitates and their coalescence in lamellae, respectively [11, 12].

It can be noted that the transformation sequence for Pb–0.08%Ca–2.0%Sm alloy is similar to those obtained for Pb–0.08%Ca alloy treated in the same experimental conditions. Nevertheless, the exothermic peak (A) is not encountered for the ternary alloy. Several explanations can be proposed: firstly, the corresponding exothermic effect on DSC curve is too weak to be detected; secondly, this heating effect occurs at the temperature lower than −5°C as shown by Bouirden et al. [6].

The samarium addition to the Pb–0.08%Ca alloy seems to lead to the shift of the transformation beginning temperature (T_i) towards the lower temperatures. More particularly, the T_B and T_C temperatures increase of 20 and 80°C, respectively. So the samarium element could accelerate the first transformations of the age hardening of the Pb–0.08%Ca alloy by decreasing the corresponding beginning temperature.

Hardness tests

Figure 2a and b give the hardness curves of the quenched Pb–2%Sm and Pb–0.08%Ca–2.0%Sm alloys at room temperature, respectively. It can be noted that Pb–2%Sm alloy does not show any hardening process after 2 ageing years at room temperature; its hardness value remains constant and equal to those of pure lead, i.e. 5.5 HV. Conversely, the hardness of the ternary alloy rapidly increases for the first days after quenching. Moreover, Pb–0.08%Ca–2.0%Sm alloy reaches after 1 month at room temperature a maximum hardness value of 14 HV, which corresponds to that obtained for Pb–0.08%Ca alloy [6].

The kinetics of the first steps of hardening process for Pb–0.08%Ca–2.0%Sm alloy can be evaluated by hardness measurements. Indeed, each transformation is characterized by a single hardness jump. So from Fig. 3, it can be detected three successive transformations. The corresponding incubation times (t_i) are reported in Table 1. The first jump is linked to the first discontinuous transformation (A) and leads to a hardness increment of 2 HV, the second one corresponds to the « puzzling » transformation (B) and permits reaching 8.5 HV, at least, the third peak can be attributed to the discontinuous or continuous precipitation of Pb_3Ca phase.

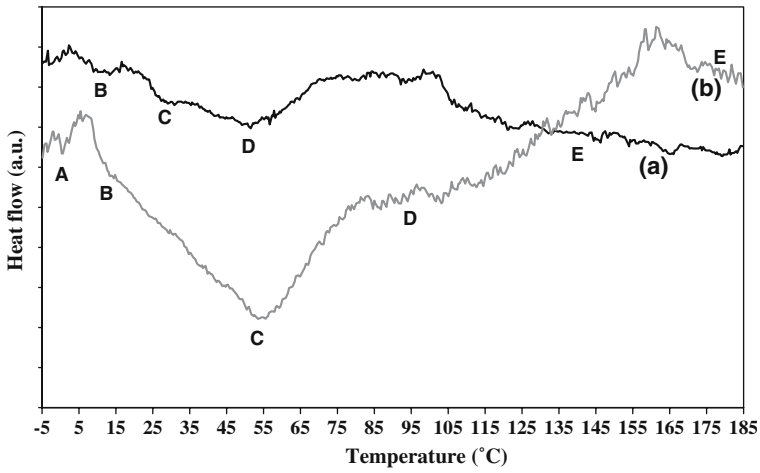

Fig. 1 DSC thermograms of the quenched Pb–0.08%Ca–2.0%Sm and Pb–0.08%Ca alloys (heating rate = 1°C · min^{-1})

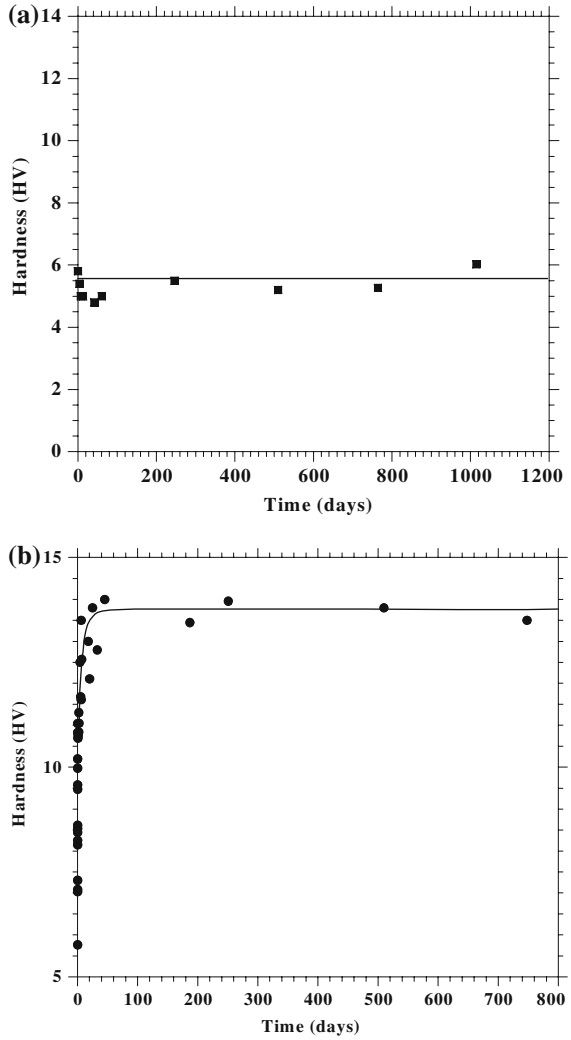

Fig. 2 Hardness evolution at room temperature of the quenched Pb–0.08%Ca (**a**) and Pb–0.08%Ca–2.0%Sm (**b**) alloys for the first discontinuous transformations of the ageing process

The comparison of incubation times (t_i) obtained for Pb–0.08%Ca and Pb–0.08%Ca–2%Sm alloys (Table 1) suggests that the rare earth element has an accelerating effect on the age hardening process. Nevertheless, the hardness jump amplitude of the first transformation appears weaker for ternary alloy than for Pb–0.08%Ca.

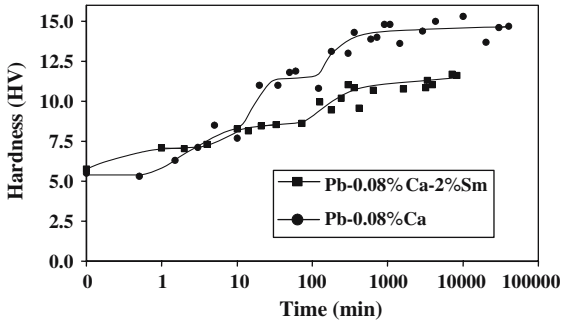

Fig. 3 Hardness evolution at room temperature of quenched Pb–2.0%Sm and of Pb–0.08%Ca–2.0%Sm alloys

Table 1 Incubation times of transformations A, B and C determined from the hardness curves of Fig. 3

Type of alloy	Incubation time of each transformation (mn)		
	t_A	t_B	t_C
Pb–0.08%Ca	1	10	120
Pb–0.08%Ca–2.0%Sm	<0.1	4	72

Microstructural characterization (TEM and SEM observations)

Pb–2%Sm alloy

The SEM observations of the quenched Pb–2%Sm alloy microstructure (Fig. 4) reveal the presence of small samarium enriched zones. Their symmetry is mainly of cubic shape. From EPMA analyses, it appears that their chemical composition corresponds to Pb_3Sm phase (Table 2).

For Pb–2%Sm alloy and pure lead, the corresponding grain size distribution are determined from a SEM micrographs. This analysis was performed with Scion Image software (Scion Image Corporation) from 300 detected particles. The results so-obtained for Pb–2%Sm and pure lead are reported in Fig. 5. For both

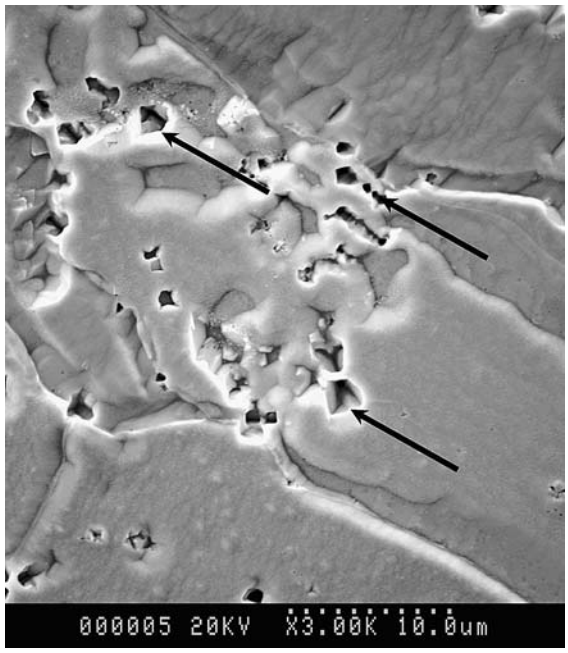

Fig. 4 SEM micrographs of the Pb–2.0%Sm quenched and aged for 1 month at room temperature after chemical attack

Table 2 Chemical composition of the precipitated phase and of the matrix of the quenched Pb–2%Sm alloy then aged for 1 month at room temperature

Characterized zone	at.% Sm	at.% Pb
Dark zone	24.88	75.12
Matrix	0.02	99.98

samples, the grain size distribution is monodispersed. Nevertheless, the ternary alloy microstructure seems to be finer: the samarium addition leads to an average grain size decrease by a 6-factor with regards to those of pure lead. Otherwise, the refinement effect of the rare earth element has been already noted by several authors [13], in particular, for Pb–60%Sn–*x*%Ce alloy.

Pb–0.08%Ca–2.0%Sm

The microstructure of the supersaturated Pb–0.08%Ca–2.0%Sm alloy after a treatment of 1 month at room temperature exhibits two samarium enriched phases (see Fig. 6): cubic shaped particles (a (5 μm) of Pb_3Sm and fine precipitates which have been characterized by transmission electron microscopy.

The chemical composition of the finer precipitates has been determined by coupling EDXS and TEM techniques. The precipitate compositions obey to the $Pb_3(Ca, Sm)$ solid solution. Moreover, the bright field TEM image of the same alloy (Fig. 7) reveals that these $Pb_3(Ca_{1-x}Sm_x)$ precipitates adopt a spherical shape ($\varnothing_m$ = 500 nm). Furthermore, Fig. 7 shows the

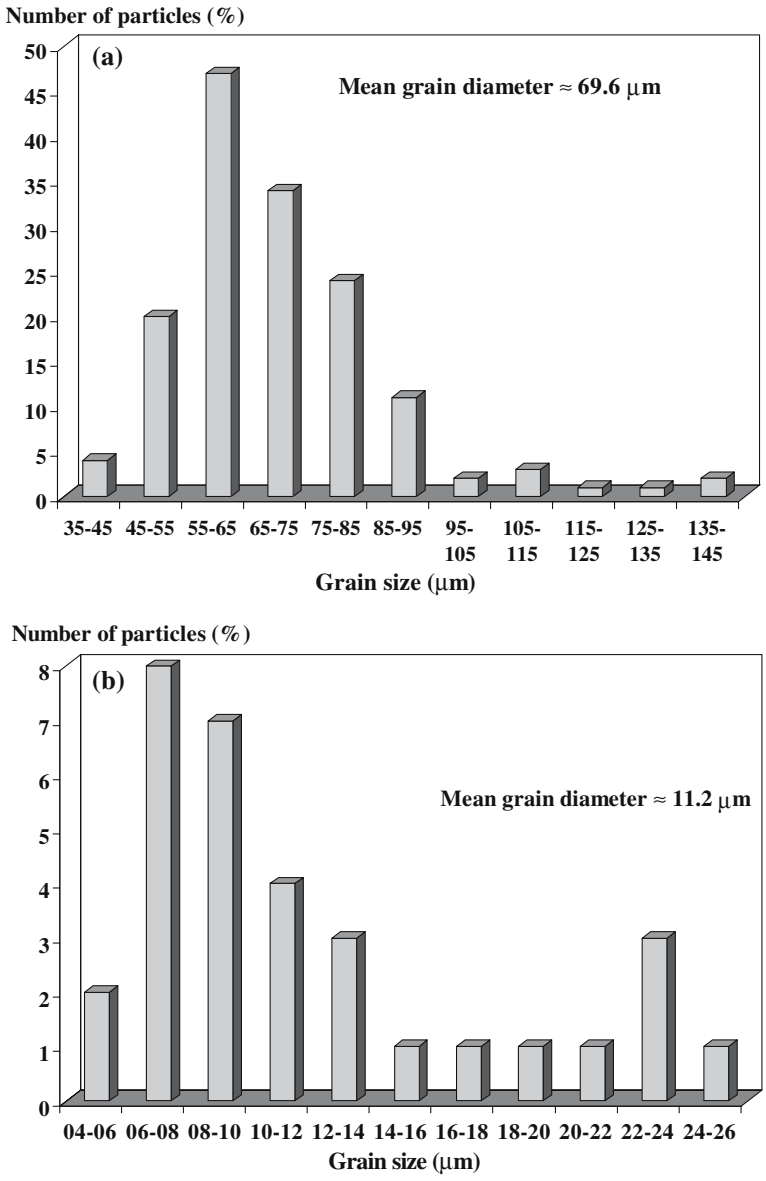

Fig. 5 Grain size distributions of pure lead (**a**) and of Pb–0.08%Ca–2.0%Sm alloy (**b**) after 1 month at room temperature

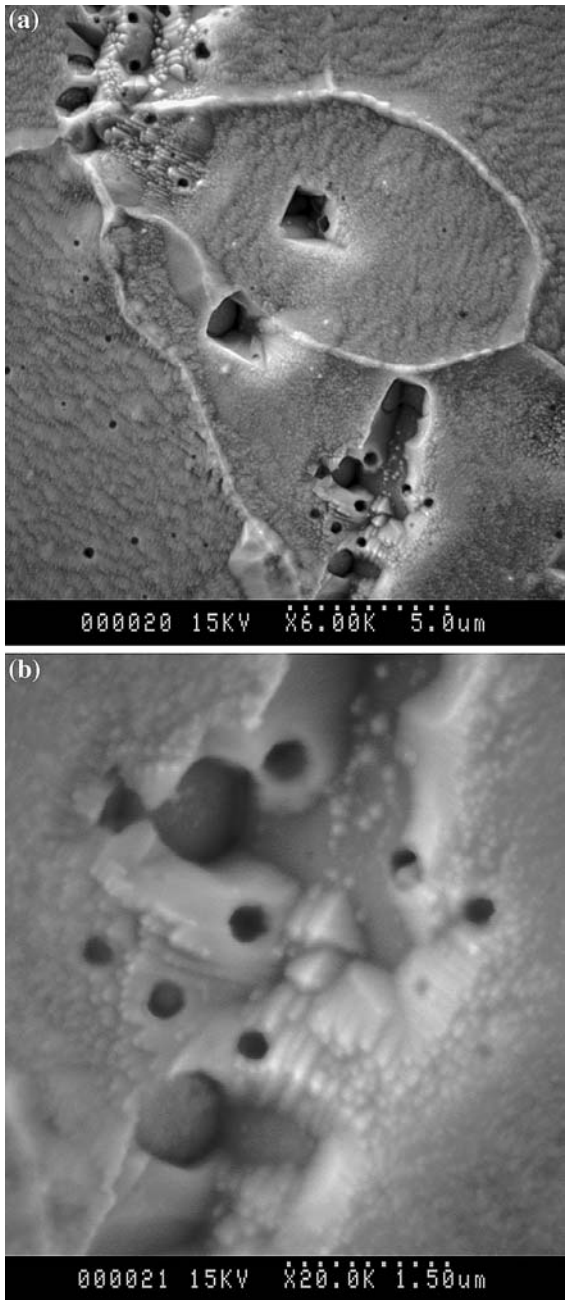

Fig. 6 SEM micrographs of the Pb–0.08%Ca–2.0%Sm alloy quenched and aged for 1 month at room temperature

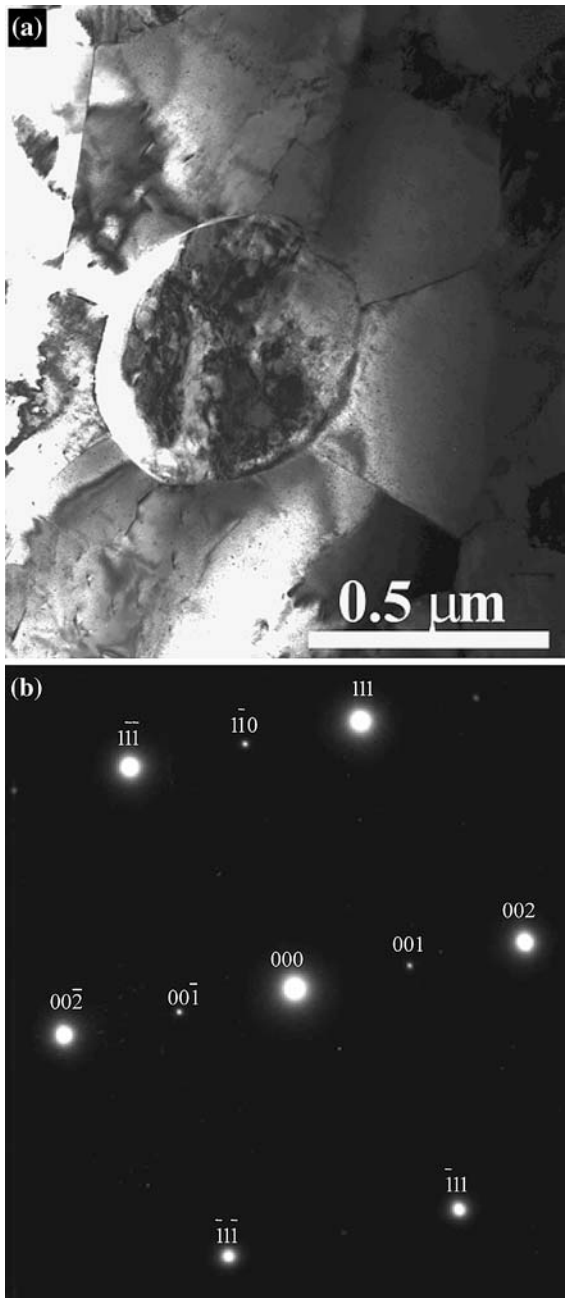

Fig. 7 TEM bright field image of Pb–0.0.8%Ca–2.0%Sm alloy quenched and aged for 10 days at room temperature (**a**) and SAED pattern of the corresponding intermetallic precipitate (**b**) (zone axis [110] of lead)

presence of a fine distribution of precipitates probably of β-phase (i.e. of Pb_3Ca). Indeed, even if the quantitative EDXS analysis of these precipitates is not possible due to their small size, it is nevertheless noted that a calcium enrichment around them exist.

These results confirm that samarium does not induce an age hardening process with a fine Pb_3Sm intermetallic precipitation. SEM observations of Pb–2%Sm alloy (see Fig. 4) indicate the formation of coarse Pb_3Sm precipitates during the quenching step. The presence of these precipitates on the grain boundaries could lead to the microstructure refinement. On this subject, the Pb–Sm phase diagram [14] which is reported in Fig. 8 gives no precise information concerning the Sm solubility in (αPb) in the temperature range (20–280°C). Indeed, we did not find in the literature any data concerning the determination of the solvus line near the lead-rich border.

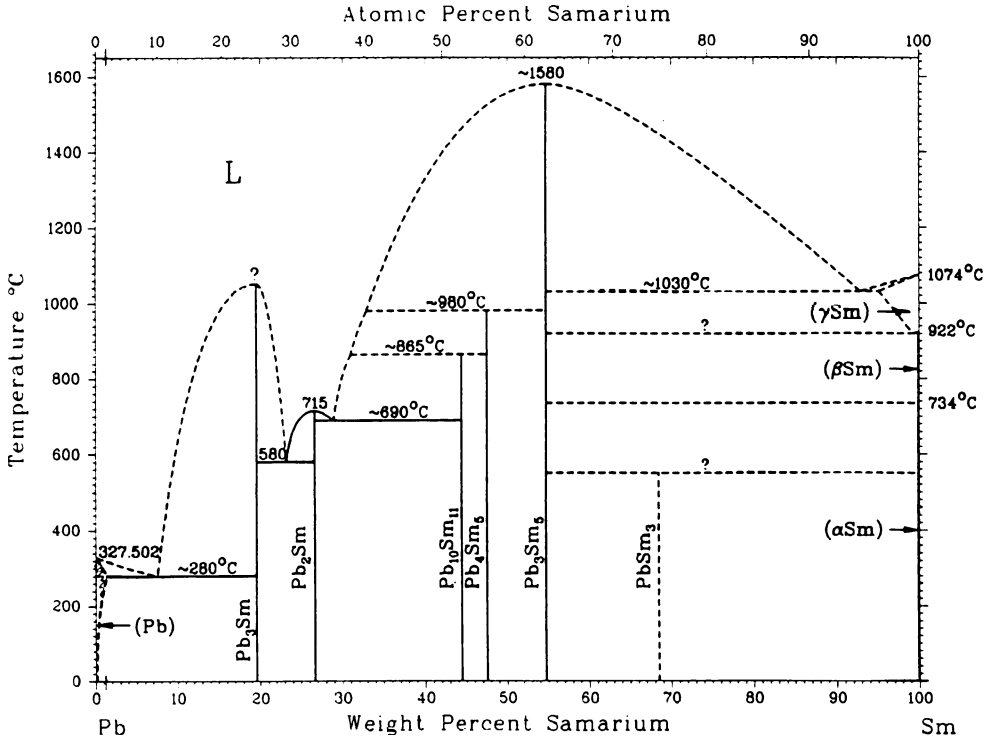

Fig. 8 Pb–2.0%Sm phase diagram available in the literature [14]

Otherwise, samarium additions do not modify the transformation sequence of the age hardening process of the Pb–0.08%Ca alloy. Nevertheless, the Pb–0.08%Ca alloy microstructure refinement due to Sm additions improves the kinetic of the first transformations of ageing by increasing their initiation site number.

Corrosion tests

Voltametry cyclic

The electrochemical behaviour of Pb–2.0%Sm is similar to that of pure lead in concentrated sulphuric acid solution [15]. The Pb–2.0%Sm alloy like pure lead shows an active domain and a large passivation plateau (see Fig. 9). On the voltammogram of the Pb–2.0%Sm alloy obtained in 0.5 M sulphuric acid at room temperature (Fig. 9), it can be noted the presence of several anodic peaks (A1, A2 and A3) which can be attributed to the lead oxidation into $PbSO_4$ at about −900 mV (A1), to the $PbSO_4$ oxidation in PbO_2 at 1250 mV (A2) and the water oxidation in oxygen at 1500 mV (A3). During the potential decrease (from about 1500 mV), two anodic peaks (A4 and A5) and three cathodic peaks called C1, C2, C3 have been detected. The anodic peaks correspond to the PbO oxidation in PbO_2 and the lead oxidation in PbO or $PbSO_4$, respectively.

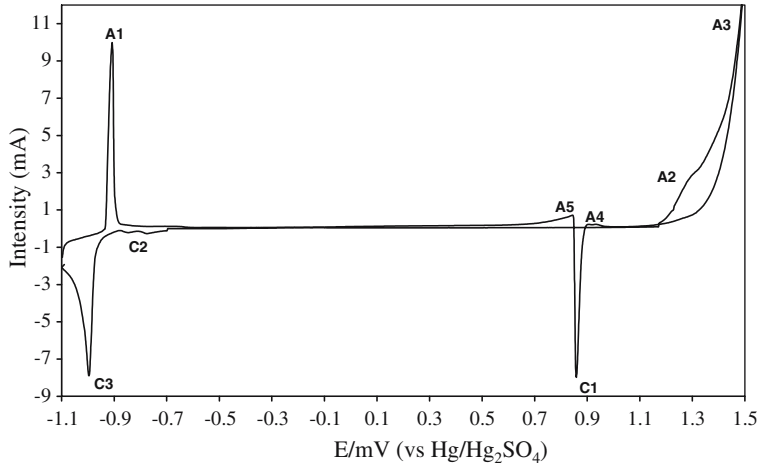

Fig. 9 Characteristic cyclic voltammograms for the Pb–2.0%Sm alloy in 0.5 M H_2SO_4 solution at room temperature (sweep rate: 1 mV · s^{-1})

The peaks C1, C2, C3 are linked to the reduction of PbO_2 in $PbSO_4$ at about 850 mV, of PbO in Pb at −800 mV and of $PbSO_4$ in lead at −1000 mV, respectively.

Nevertheless, the oxygen surtension is shifted towards the higher potential values in presence of Sm: the Pb–2.0%Sm alloy shows an oxygen surtension value of 1260 mV as opposed to 950 mV obtained for pure lead [15] in the same working conditions. The favourable role played by the rare earth has been already detected by Wie et al. [16] during the characterization of electrochemical properties of Pb–Ca–Ce or Pb–Sb–Ce alloys.

Polarisation tests

The overcharge conditions are simulated by a polarisation test at 1.5 V for 5 days in 5 M sulphuric acid

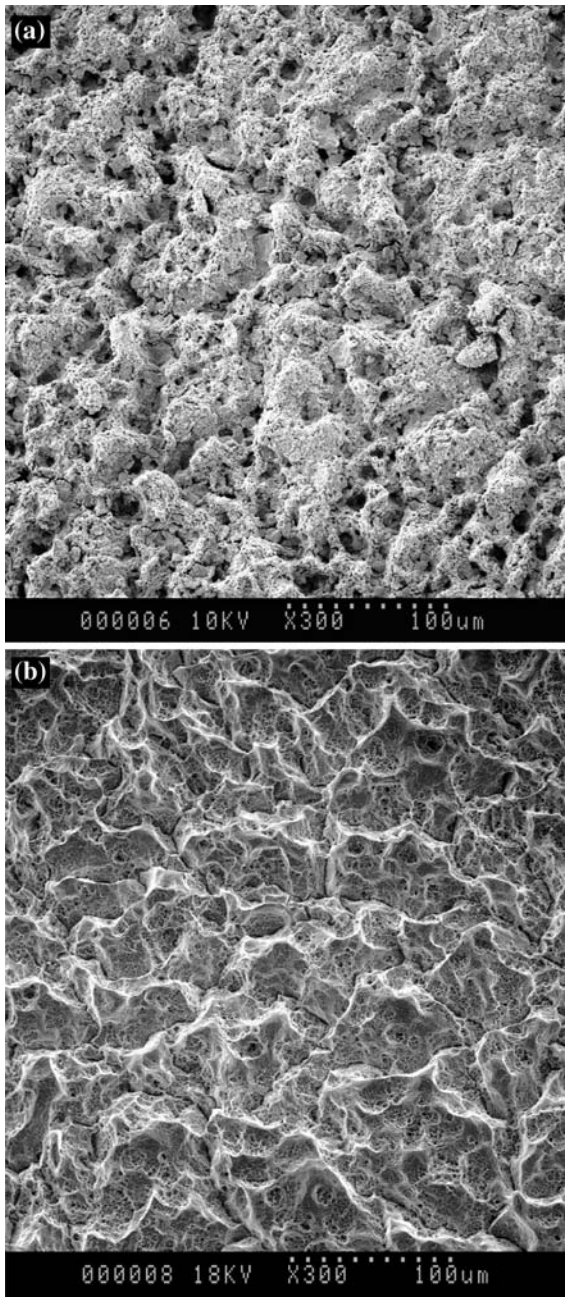

Fig. 10 SEM micrographs of the Pb–2.0%Sm alloy surface after 5 days at 1.5 V in 5 M H_2SO_4 at room temperature: with the corrosion products (**a**) or without the corrosion products (**b**) (suppressed by hydrazine inversion)

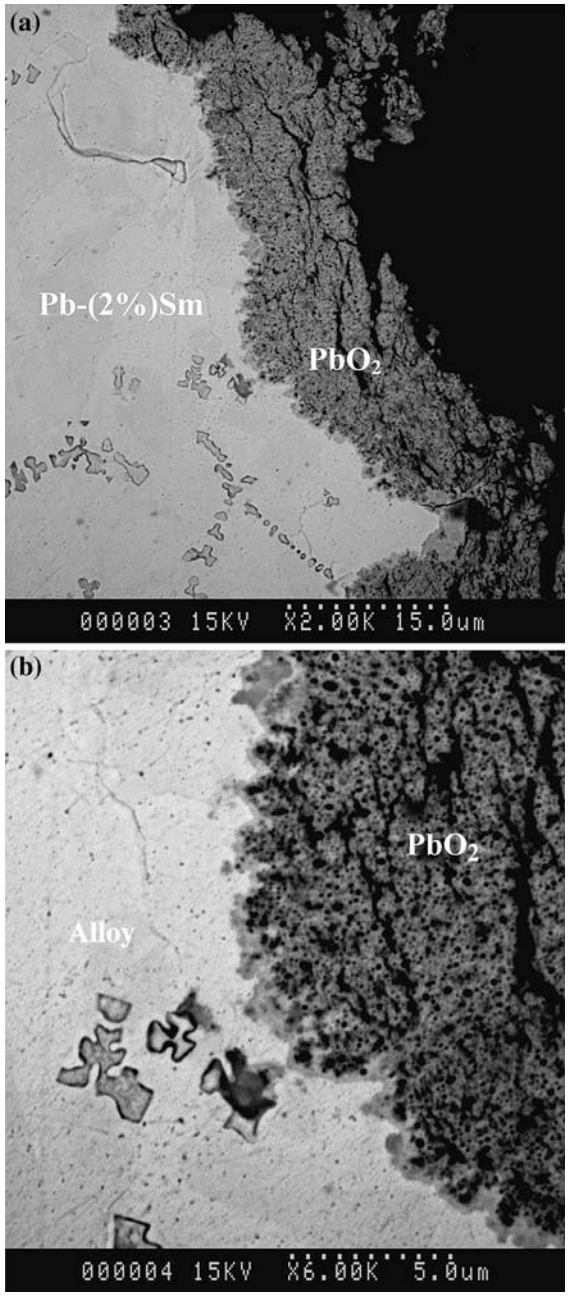

Fig. 11 Metallographic cross-section at different magnifications (**a**) and (**b**) of the Pb–2.0%Sm alloy after 5 days at 1.5 V in 5 M H_2SO_4 at room temperature

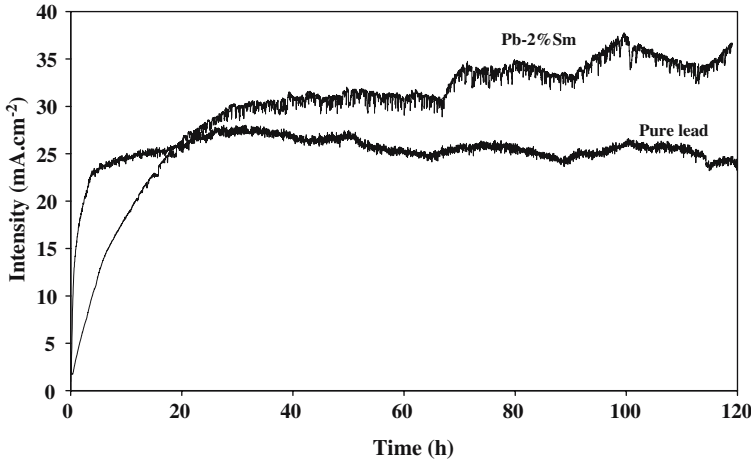

Fig. 12 Current evolution during a potentiostatic oxidation for 5 days at 1.5 V (vs. Hg/Hg_2SO_4) in 5 M H_2SO_4 solution at room temperature for pure lead (**a**) and Pb–2.0%Sm alloy (aged 1 month at room temperature after quenching)

maintained at 20°C. SEM observations (Fig. 10a) reveal the presence of micro-cracks in the corrosion layer surface due to the oxygen release from the lead alloy/lead oxide interface. The Pb–2%Sm alloy undergoes a severe attack that is well characterized by a preferential intergranular corrosion as shown in Fig. 10b.

A cross section observation of the same sample (Fig. 11a) confirms the preferential corrosion at the grain boundaries. At the PbO_2/Pb–2%Sm alloy interface, a dense and thick layer of lead monoxide is detected from chemical analyses performed with EPMA technique (Fig. 11b). Numerous microcracks can be observed through the corrosion layer indicating the existence of an important oxygen release during the polarisation test.

The weight loss measured for Pb–2%Sm alloy, i.e. 36.4 mg cm^{-2}, is higher than that determined in the same conditions for pure lead (23.7 mg cm^{-2}). Consequently, it seems that the Sm addition significantly decreases the lead corrosion resistance in sulphuric acid.

Moreover, $i = f(E)$ curves (Fig. 12) confirms that the corrosion phenomenon is more important on the Pb–2%Sm electrode. The observed current variations are probably due to the oxygen release which induces the lead oxide layer micro-cracking and quasi-simultaneously to the re-oxidation of the electrode.

Conclusion

The characterization of the metallurgical transformations for both Pb–2%Sm and Pb–0.08%Ca–2%Sm was performed using several complementary techniques such as transmission electron microscopy or differential calorimetry. The samarium element seems to accelerate the kinetics of the first discontinuous transformations by refining the lead microstructure or by increasing their initiation site number.

Otherwise, the electrochemical tests performed in the battery overcharge conditions have clearly shown that the corrosion behaviour of pure lead decreases in presence of samarium. This result is also due to the microstructure refinement and, consequently, to the reinforcement of the intergranular corrosion. Nevertheless, the rare earth addition appears to play a favourable role by increasing the oxygen surtension in comparison with the pure lead.

At last, some recent works made in the laboratory [17] tend to show that the rare earth additions (La, Ce) to Pb–0.08%Ca or Pb–0.08%Ca–x%Sn alloys increase the mechanical anchorage of the corrosion layers in the potential cycling conditions. Indeed, the better adherence of PbO_2 and PbO layers obtained in these conditions is probably linked to the presence of an intermediate $Pb_xTR_yO_z$ oxide layer at the inner interface.

Acknowledgements The authors would like to acknowledge Renaud PODOR (Laboratoire de Chimie du Solide Minéral, UHP Nancy I, France) and Gwenaelle Toussaint (Site de Recherches et Développement EDF, Moret sur Loing, France) for their technical help during this study.

References

1. Torralba M (1977) J Power Sources 1:301
2. Rose MV, Young JA (1976) In Proceedings of the 5th lead international conference, lead development association, vol. 5. Pergamon Press, Oxford, p 37
3. Hilger JP, Boularhouf A (1990) Mater Character 24:159
4. Miraglio R, Albert L, El Ghachcham A, Steinmetz J, Hilger JP (1995) J Power Sources 53:53
5. Takahashi K, Yasuda Y, Hasegawa H, Horie S, Kanetsuri K (1995) J Power Sources 53:137

6. Bouirden L, Hilger JP, Hertz J (1991) J Power Sources 33:27
7. Myers M, Van Handle HR, Dimartini CR (1974) J Electrochem Soc 121:1526
8. Vilasi M, Steinmetz J, Steinmetz P (1989) Mater Sci Eng A 120–121:161
9. Bourguignon G (2003) Thesis of University of Nancy I. (In French)
10. Villars P, Calvert LD (1985) Pearson's handbook of crystallographic data for intermetallic phase. American Society for Metals, USA
11. Hilger JP (1998) J Power Sources 72:184
12. Maitre A, Bourguignon G, Fiorani JM, Steinmetz J, Ghanbaja J, Laillier P (2003) Mater Sci Eng A 340:103
13. Ying ZH, Hongyuang F, Yiyu Q (1994) Mat Res Soc Symp Proc 323:137. (In chinese)
14. Moffatt WG (1978) The handbook of binary phase diagrams. Genium Pub. Corp., New York, USA
15. Rocca E, Steinmetz J (1999) Electrochem Acta 44:4611
16. Wie J, Zhao L, Sun F, Yang H, Chu D (2003) Zhongguo Youse Jinshi Xuebao 13:497
17. Bourguignon G, Maitre A, Rocca E, Steinmetz J. (To be published)